Applied Physics A (2020) 126:397
https://doi.org/10.1007/s00339-020-03595-2

Applied Physics A
Materials Science & Processing

Impact of light soaking on absorber and buffer layer in thin film solar cells

Atul Kumar[1] · Pranay Ranjan[2]

Received: 31 January 2020 / Accepted: 29 April 2020 / Published online: 8 May 2020
© Springer-Verlag GmbH Germany, part of Springer Nature 2020

Abstract
Light soaking in thin film solar cells shows both beneficial and detrimental impact on efficiency depending upon the absorber–buffer pair. We here numerically simulated the advantageous and detrimental impact of light soaking behavior as experimentally observed in the literature by utilizing suitable defect models for the two cases, respectively. The proposed models are based on the photoconductivity and metastable photo-induced activity of absorber and buffer layers. It is observed that light soaking in absorber layer vis-a-vis photo-induced defect in absorber is beneficial for device performance. Photo-generated defect in absorber acts as hole doping which is turn enhance the built-in voltage. The photoconductivity of the buffer layer is detrimental to the device performance. The photo-generated defects in the buffer cause lowering of fill-factor, current, accelerate interfacial recombination and depreciate overall efficiency.

Keywords Light soaking · Metastability · Acceptors defects · Thin film solar cells

1 Introduction

Thin film solar cells of abundant and low-cost material are potential future energy source. However, these solar cells have much of the technological optimization still to be perfected and controlled before it could overtake as stable energy source. Optimization is challenging due to variety of involved variable such as radiation, thermal, atmospheric stresses in addition to non-uniformities related to thin film hetero-structures fabrications [1]. One such issue relating the performance is the light soaking behavior of thin film solar cells of CIGS [2–9], CdTe [10], CZTS [11, 12]. This phenomena cause efficiency increase after light soaking for some combination of absorber–buffers, e.g., CIGS-ZnS [5]. The same light soaking effect shows efficiency decrease for some combination of absorber–buffer like CIGS-CdS [13], etc. Other technologies like hybrid and organic solar cell [14] also show efficiency variation with light soaking. A solar cell device upon prolonged exposure to light has small transient variation in efficiency. The efficiency variation upon light soaking significantly affects the long-term power output and more importantly have associated challenges of lifetime/stability of solar cell. The slight decay in efficiency accumulates to significant power losses and revenues losses to the large-scale installers with main perspective as profitability. Thus, it becomes necessary to figure out deriving causes of detrimental effect of light soaking and avoiding them. Photoconductivity and low bandgap of buffer layer are one of the possible causes for the light-dependent behavior as reported in the literature [15]. For most of the thin film solar cells CdS is the standard buffer layer, which has the band gap of 2.4 eV. Due to this bandgap value lying in UV–Visible region, the buffer layer can absorb significant portion of incident solar spectrum. This will generate photo-carrier in the buffer layer, which will alter the initial charge distribution at the interface. Similarly, a wide bandgap buffer layer like ZnO (bandgap 3.3 eV) will pass the most of incident spectrum, to be absorbed by the absorber layer. This in turn may generate additional acceptors state in the absorber layer. These photo-induced metastable defect states in absorber, buffer and absorber/buffer interface possibly vary efficiency. Some report highlighted the chemical temporal changes in buffer under light illumination causing light soaking variation in performances of device [9]. Exact cause for light soaking variation in performance could be

✉ Atul Kumar
atul.pph14@iitp.ac.in

[1] Department of ECE, KL University, Guntur, Andhra Pradesh 522502, India

[2] Department of Physics, UAE University, Abu Dhabi 15551, United Arab Emirates

case dependent, but majorly it is the metastable defects generated in absorber and buffer under illumination. The photo-induced carriers built-up by light soaking in the absorber/buffer layer; this transient carrier density modifies the band banding and alters charge transport and the interface recombination [15–17]. The light soaking phenomena alters recombination near to junction, controlling voltage output of the device and charge transfer at junction controlling the current output of the device. The transient light dependences need to be optimized for effective high performance of the device. Here, we present a possible defect scenario replicating the two facets of light soaking phenomena in thin film solar cells using 1D simulation. Light soaking generates additional carriers [3, 4] alter mobility [4], resistance [4], defects states [11], electric field, and band banding. These aspects have implicit interdependence and effect on photovoltaic activity. Thus, a simulation-based study becomes necessary to explicitly reveal the ramification of light soaking behavior on performance and pinpointing causes responsible for such observations. Suitable defect models for efficiency enhancement and decrement corresponding to light soaking in absorber and buffer, respectively, are explored.

2 Defect model simulating light soaking

A realistic model of thin film solar cell is simulated in SCAPS-1D version 3.3.02. One can replicate our device using material parameters given in Table 1 in SCAPS 1D which is available from University of Gent [18]. More detail pertaining to this 1D electrostatic simulator can be found in the references [19–24]. Baseline model is simplistic with neutral defects and moderated back contact barrier. The detailed parameters and device specification are summarized in Table 1. Baseline structure is $pn^{+}n^{++}$ type abrupt junction as this is the configuration of thin film solar cells including CdTe, CIGS, CZTS. Bandgap value of 1.2 eV is utilized for baseline device as it is the optimum values for the most of the devices (CIGS, CZTSSe). Thickness, dielectric constant, absorption coefficient is utilized as reported for these materials in the literature. High value of surface recombination velocities (10^5 cm/s) to keep simulation results realistic. SRV values of some thin film solar cells such as CdTe are in the range of 10^5–10^6 cm/s [25], and that of CIGS lies in range 10^5-10^6 cm/s [26]. Low SRV values show high efficiency, and high SRV values lower efficiency. We have taken high SRV values in our simulation to avoid over-estimation of efficiency. Thermal velocities values for electron and hole are given by Eq. (1); there room temperature values are 10^7 cm/s [27].

$$V_{\text{th}} = \sqrt{\frac{3kT}{m^*}} \tag{1}$$

The density of state in the conduction and valence band is given by Eq. (2) [27]

Table 1 Detailed description of material parameters utilized to model a realistic thin film device [20]

Parameters	Absorber	Buffer	Window
Thickness (μm)	0.5	0.05	0.5
Bandgap (eV) (E_g)	1.2	3	3
Electron affinity (eV) (χ)	4.5	4.4	4.55
Dielectric permittivity (ε)	10	10	9
Electron/Hole thermal velocity (V_{th}^e)/(V_{th}^p) (cm/s)	10^7	10^7	10^7
Electron/hole mobility (cm^2/Vs) (μ_e)/(μ_h)	50	50	50
Donor/Acceptor density, N_D/N_A (cm^{-3})	10^{16}	10^{18}	10^{19}
Absorption coefficient (cm^{-1})	10^5	Wavelength dependent as given in inbuilt SCAPS file	Wavelength dependent as given in inbuilt SCAPS file
Surface recombination velocity electron/hole (cm/s)		10^5/10^7	
Work function of back contact (eV)		5.35	
Defects for Model 1			
Acceptor defect density (cm^{-3}), N_t 10^{14}–10^{18} Defect level E_t above E_V 0.1–0.5 eV			Within absorber layer
Defects for Model 2			
Acceptor defect density (cm^{-3}), N_t 10^{14}–10^{18} Defect level E_t above E_V 0.1–0.5 eV			Within buffer layer

$$N_{c/v} = \sqrt[3]{\frac{2\pi m^* kT}{h^2}} \quad (2)$$

We first showed the effect of illumination on baseline model. The 1D drift diffusion simulations reveal the illumination dependence transient behavior for a simplistic baseline device. The band diagram plotted in Fig. 1a is for the low illumination intensity. Fig. 1b shows the band diagram for high illumination intensity. The Fermi level corresponding to electron (E_{fn}) and hole (E_{fp}) are visibly dissimilar in the two case of Fig. 1a, b. The difference in the slope of the conduction band (E_C) or the valence band (E_V) is shown by first derivative of the E_C for the two illumination intensity in Fig. 1c. These illumination-dependent changes will be intensified for device with defects [28, 29]. This baseline model is augmented with defects to show the positive and negative effects corresponding to the light soaking behavior. Model 1 corresponds to the defect scenario, which enhanced the performance under illumination. Model 2 corresponds to the defects, which lower the efficiency under illumination. Table 1 summarizes these two defect models. Light soaking in absorber layer will generated additional states corresponding to the acceptor defect. This scenario occurs in absorber with wide bandgap buffer layer. Under prolonged illumination or light soaking the metastable acceptor level is generated in the absorber layer. Defect corresponding to this scenario is called model 1 and is schematically shown in Fig. 2a. This transient acceptor concentration will decay down under dark. This photo-generated carrier concentration acts as additional hole doping in the absorber which is discussed in following sections. Model 1 type light soaking results in large increment in V_{OC} than other parameters [30, 31]. The persistent photoconductivity of buffer layer will generate photo-induced carrier concentration across the buffer layer, which will alter the band banding at the absorber/buffer interface. Photoconductivity effect of buffer layer with photo-generated defects in buffer [5, 11] is taken as model 2. A schematic depiction is shown in Fig. 2b for the physical scenarios of model 2. The numerical values of defects as utilized to simulate the positive and negative light soaking behavior are summarized in boxes for the two cases in Fig. 2. Two models are simulated along with the baseline model to reveal the nature of light soaking behavior causing enhancement and decrement in efficiency. The ramifications of these two physical scenarios are discussed in detail in next section.

3 Results and discussion

Efficiency-space plot of baseline device with defect scenario of model 1 and model 2 is plotted in Fig. 3. A simulation is run over a range of acceptor defect density and energy level above E_V variation in absorber layer for the case of model 1. Contour plot shows the higher efficiency region for the model 1 to have a positive impact on the efficiency. Shallow levels near to the E_V in the absorber with high density are the prerequisite for the model 1 acceptors defects to have a high positive impact. The model 2 that represents the photo-generated defect in the buffer layer shows efficiency decrease with the higher density of photo-generated acceptor defect with shallow level benign then deep defects. Efficiency raises from 18% mark to 20% for the case of model 1 and it falls from 18% mark to 16% for the case of model 2. This contour plot implicitly established that the acceptor defect in absorber layer (Model 1) enhances performance from base level and the photo-generated acceptor defect in the buffer (Model 2) lower performance.

The comparative current–voltage (I-V) characteristic of the baseline and with incorporation of model 1 and model 2 is shown in Fig. 4. The baseline device has absorber hole doping of 10^{16} cm^{-3} and buffer electron concentration of 10^{18} cm^{-3}. The defects model 1, I–V have higher V_{OC} than the baseline device. The acceptor defect have effectively increased the hole doping thus the built-in voltage and open-circuit voltage output than the baseline device as seen in

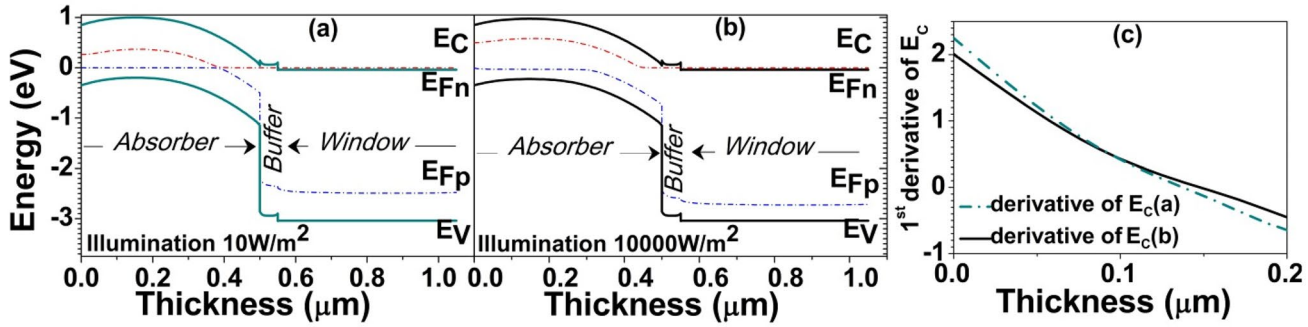

Fig. 1 (Color online) **a** Band diagram of the device under low illumination intensity, **b** the band diagram in high Illumination intensity, **c** The first derivative of conduction band level showing the illumination change in the band diagram

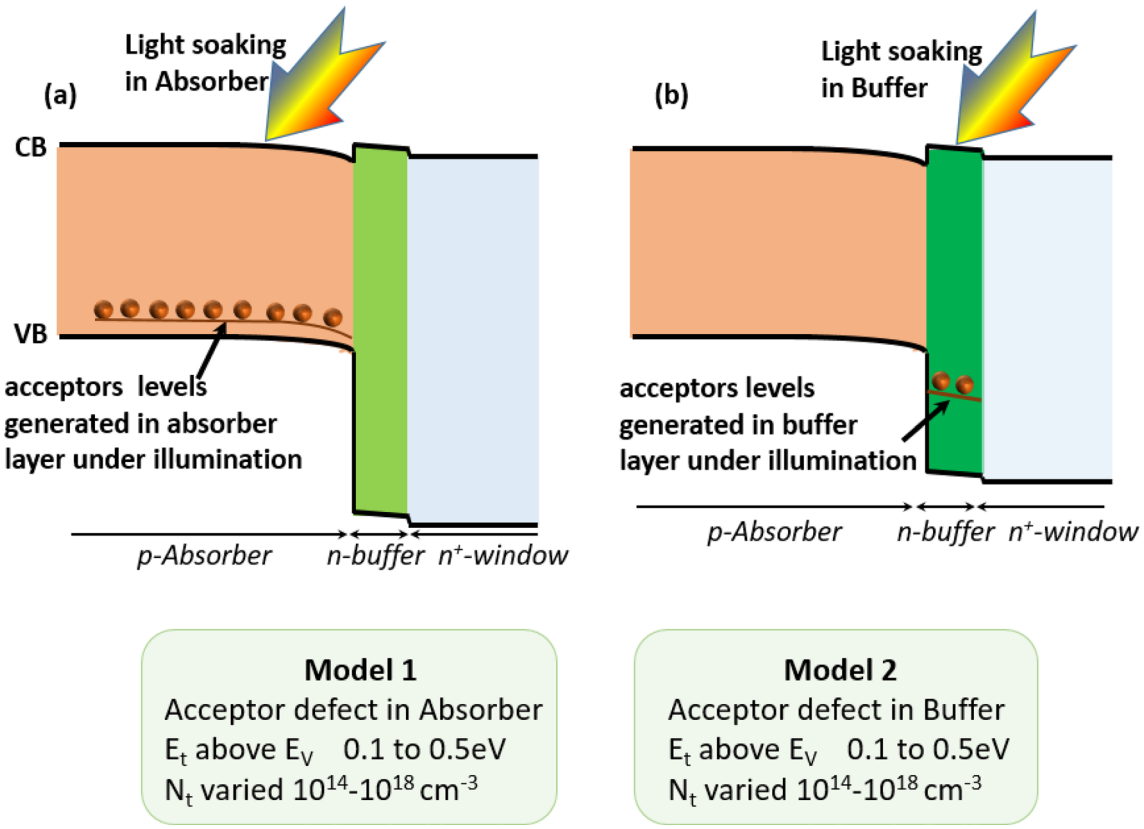

Fig. 2 (Color online) **a** Schematic representation of the defect scenario of Model 1 showing the acceptors defect level in the absorber layer generate under light exposure, with wide bandgap buffer counterpart. Description of defects in Model 1 is shown in box below. **b** Schematic representation of Model 2 whereby defect level are generated in buffer layer under light exposure. Description of defects in Model 2 is shown in box below

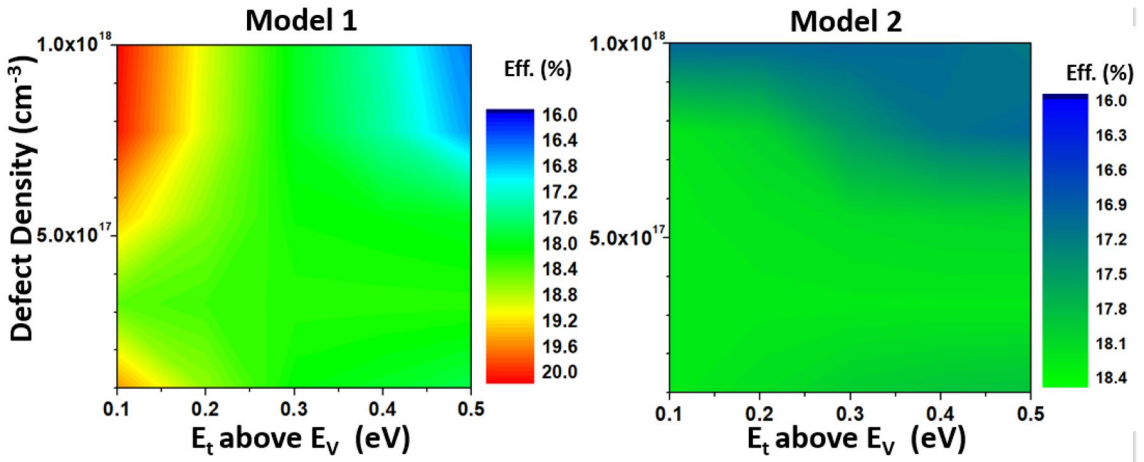

Fig. 3 (Color online) 2D contour plot of the efficiency as a function of acceptor defect density and defect energy level within the forbidden gap for the Model 1 and Model 2, respectively

Fig. 4. The model 2 has acceptor level in the buffer layer, showed lower current and fill factor (FF) than the baseline. Acceptor defect in buffer has increased recombination thus lowering the overall efficiency as compared to the baseline device. FF of the baseline device increase with the incorporation of defect of model 1 and decreases for the model

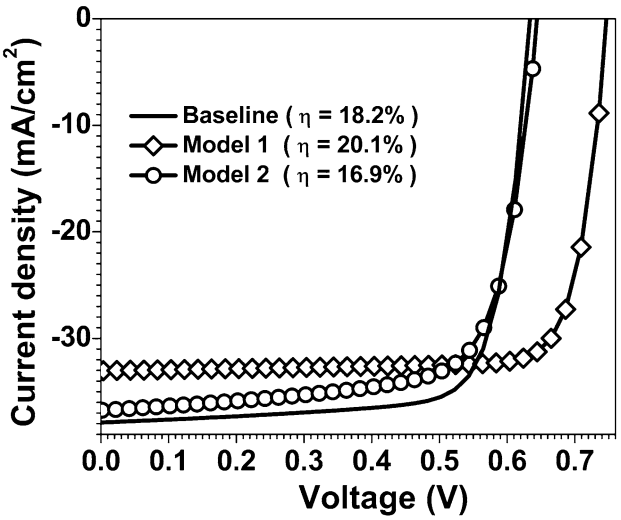

Fig. 4 (Color online) The comparative I-V characteristic for the baseline, Model 1 and Model 2 defect scenarios. Arrow in colored region shows the increase and decrease in V_{OC} and J_{SC} for Model 1 and Model 2, respectively

2. Model 1 simulates the positive impact of light soaking phenomena and model 2 simulates the negative impact of the light soaking phenomena.

The solar cell performance parameters of efficiency, open-circuit voltage and fill factor (FF) increase with the acceptor density in absorber layer. The acceptor defect density is varied from 10^{14}–10^{18} cm^{-3}. Figure 5a shows the rise in efficiency from the level of baseline model with the increase in the acceptor density in absorber layer. There is improvement in the V_{OC} values with the acceptor defect density. Fill factor rises with acceptor defect concentration as shown in Fig. 5b. It is observed that the current falls with the increasing acceptor density. The short-circuit current J_{SC} decreased considerately from the 37.8 to 33 mA/cm^2 an approximate fall of 15%. The specific reason for the loss in current is discussed in next section. Overall effect of acceptor density is the positive increase in the performance.

The acceptor density in the buffer layer showed a negative impact on the overall device performance. Figure 6a shows the decay in the efficiency from the level of baseline device with the increase in the acceptor density in buffer layer. The acceptor defect density in buffer layer is varied from 10^{14} to 10^{18} cm^{-3}. However, though V_{OC} values observe to mildly improve with the acceptor defect density as shown in Fig. 6a, fill factor and current both fall with increasing acceptor concentration in buffer layer as shown in Fig. 6b. This negative impact of model 2 is discussed in simulation of interfacial recombination and band diagram simulation. Both the model start at the level of baseline performance and the performance increases for the model 1 and decreases for model 2 with increasing acceptor defect concentration in absorber and buffer, respectively.

Batch simulations are run in the SCAPS, to compare the bulk recombination current within the device for the two cases. Bulk recombination is higher in case of model 1as plotted in Fig. 7a. The defect is across the absorber and

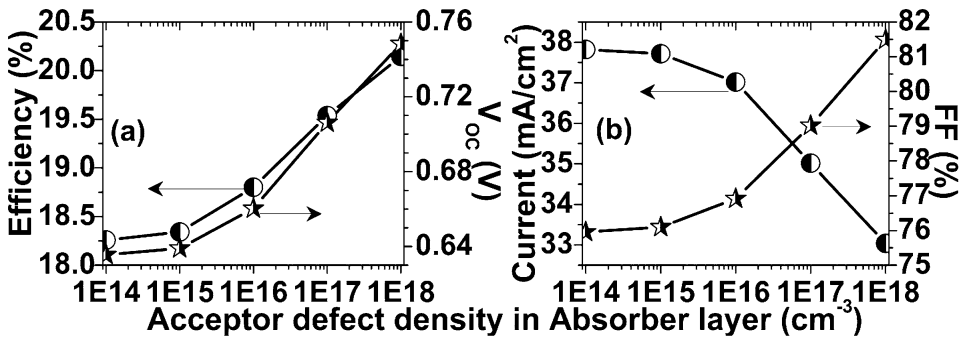

Fig. 5 (Color online) **a** The increase in performance parameter of efficiency and V_{OC} with acceptor defect and **b** current and FF variation as a function of acceptor defect density for Model 1

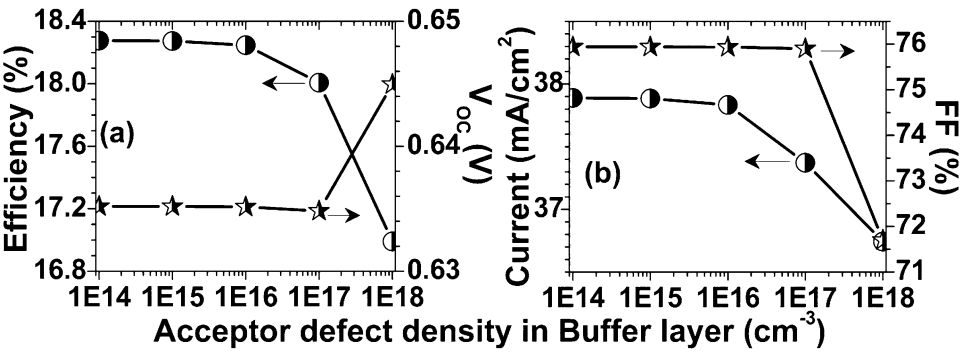

Fig. 6 (Color online) **a** The performance parameter of efficiency and V_{OC} and **b** current and FF as a function of defect density for the case of Model 2

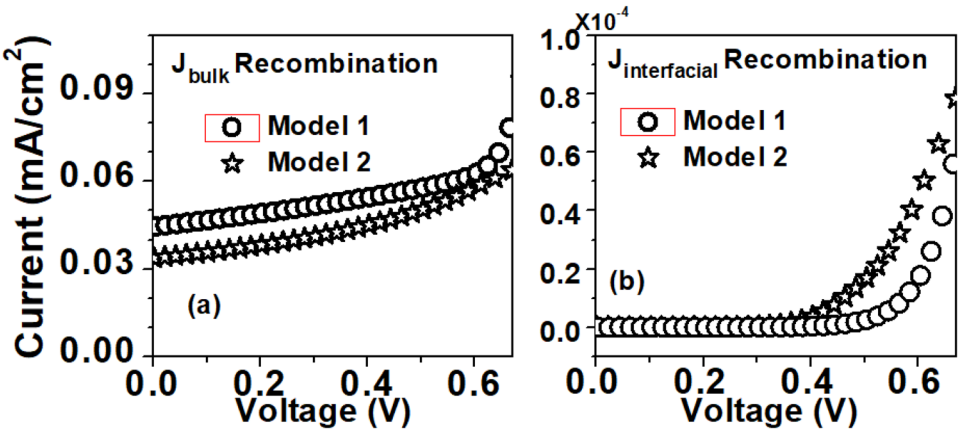

Fig. 7 (Color online) **a** The bulk recombination current in the device and **b** interfacial recombination current in the device for the case of Model 1 and Model 2 as a function of voltage

buffer width. The absorber width is much larger than the buffer, thus higher bulk recombination for absorber, i.e., model 1. This has lowered the J_{SC} values by 35% as shown in Fig. 5b. However, the buffer defects have accelerated interface recombination as shown by the interfacial recombination current in Fig. 7(b).

The spatial variation in band diagram for model 1 with different defect concentration is plotted in Fig. 8a–c. The band diagram changes drastically for higher acceptor concentration. The acceptor defect has increased the built-in voltage (V_{bi}). This increased built-in voltage is the reason for higher V_{OC} values observed for the case of model 1. The acceptor defect in model 1 is effectively acting as a hole doping in the absorber layer. However, at this increased hole doping in bulk, the bulk recombination is increased. Also the space charge width is decreased thus lowering the current collection. The bulk recombination plotted in Fig. 7a confirms higher recombination in bulk is for the model 1 and is the reason for lower J_{SC} values. Bulk recombination comprises of radiative, SRH and the Auger recombination in the absorber layer. For the case of model 2 when acceptor defects are generated in buffer layer the band banding is shown in Fig. 8d–f. The band diagram for low defect density is similar but drastically changes for higher defect density as

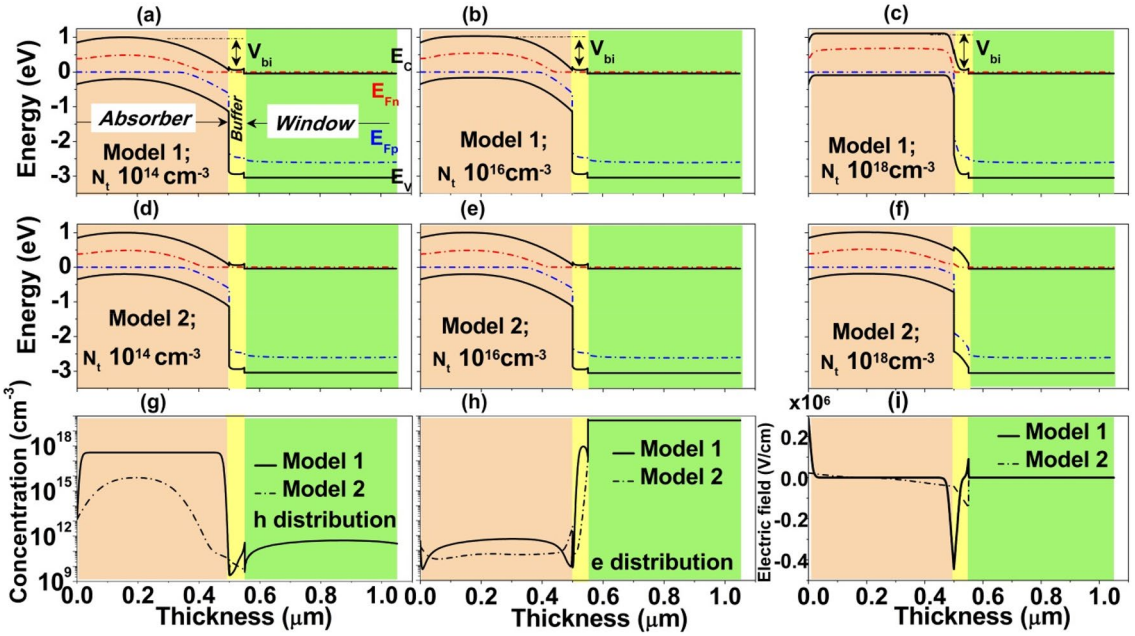

Fig. 8 (Color online) **a–c** The band diagram for varied acceptor density in case of Model 1; **d–f** band diagram for Model 2 with variation in defect density; **g** The hole distribution profile across the width of the device for Model 1 (continuous line) and Model 2 (dash-dot line); **h** The electron concentration variation across the width of the device for Model 1 (continuous line) and Model 2 (dash-dot line); **i** the electric field profile across the absorber/buffer junction for Model 1 (continuous line) and Model 2 (dash-dot line)

seen in Fig. 8f. The higher defect concentration buffer layer has strong band banding within buffer. This condition has maintained the V_{OC} even for the high defect. As compared to the baseline current and FF values in model 2 has degraded. The higher interfacial defect for model 2 is reflected in the lower J_{SC} and FF. The carrier distribution profile as a function of defect concentration for the two models is comparatively depicted in Fig. 8(g). The hole doping in the baseline device is 10^{15} cm^{-3}. It is depicted in Fig. 8(g) that the hole concentration is higher than the baseline doping. This high hole concentration is throughout the absorber bulk is due to the acceptor defects generated in the illumination. The acceptor defects in *p* type layer effectively act as hole doping. This higher carrier concentration in the absorber layer resulted in the high bulk recombination in absorber layer. Figure 8h shows the electron distribution profile for the two models. The electrons concentration in the buffer layer is lowered by the acceptor defects (taken to illumination generated defects). Figure 8i shows the electric field variation in the device for the 8c and 8f. The electric field for the model 1 is observed at the *p*-*n* (absorber–buffer) interface. The electric field at the n–n^+ (buffer-window) is observed for the model 2 case. Therefor high interfacial recombination at the *p*-*n* interface is occurs for model 2, which lowers the current and FF and thus efficiency.

One more analysis to establish the hole doping by metastable defects due to light soaking is simulated as capacitance–voltage (C–V). Applied negative voltage corresponds to reverse bias shows the geometrical capacitance of device, which increase under forward bias in Fig. 9. Capacitance for model 1 is higher due to high acceptor defects concentration in absorber (corresponds to photo-generated carrier in light soaking) shown by the line with open circle in Fig. 9. The lower depletion region thickness as shown in Fig. 8c will result into high junction capacitance for model 1. The capacitance variation for baseline device is shown by open square symbol, model 1 by open circle and model 2 by open diamond, respectively. Inset shows the Mott–Schottky plot calculated from the *C*–*V* data. Mott–Schottky plot show a liner variation for reverse to forward biasing meaning a uniform doping profile. The varied slope of $1/C^2$ versus V corresponding to the doping profile in the various case, which is given by $\frac{1}{C^2} = \frac{2(V_{bi}-V_a)}{q\varepsilon N_A}$ where symbols have usual meaning. Upon light soaking the device shows increase in capacitance values and a linear Mott–Schottky profile for efficiency enhancement behavior of the light soaking [2]. A similar behavior is simulated by model 1 which replicates the efficiency enhancement behavior of the light soaking.

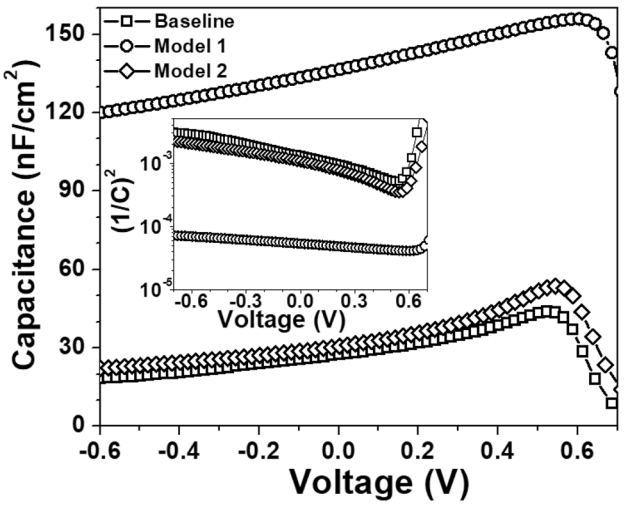

Fig. 9 (Color online) The capacitance–voltage (*C*–*V*) plot of the device for baseline, Model 1 and Model 2. Inset shows the Mott–Schottky plot corresponding to the *C*–*V* curve

Under prolonged illumination or light soaking absorber layer will generate additional states and metastable acceptor levels in the absorber layer. This transient acceptor concentration will decay down when illumination is removed. Figure 2a schematically shows this defect scenario as model 1. This photo-generated carrier concentration acts as additional hole doping in the absorber which is beneficial for device performance. On the other hand a low bandgap *n*-type buffer layer will absorb significant solar spectrum and generates electrons and holes pairs within buffer layer. This addition defects levels near the valence band in the buffer layer alters the band banding at the absorber/buffer interface and are detrimental to device performance. A schematic depiction is shown in Fig. 2b for the physical scenarios of defects in buffer layer as model 2. A comparison of band banding for model 1 and model 2 in Fig. 8c, f shows the extent of band banding at the absorber/buffer interface and built-in voltage variation. We consider the two scenarios as two defect models and replicated the experimentally observed beneficial and detrimental aspect of light soaking. These two models along with the baseline model implicitly depict enhancement and decrement in efficiency from the baseline level as shown in Fig. 4. Finally the detrimental aspect of light soaking phenomena related to buffer layer in thin film solar cells could be addressed by (a) suitably thin buffer layer of high bandgap; (b) utilizing a suitable superstrate structure. Employing a suitable device configuration, negative aspect of photoconductivity of buffer layer could be suppressed and efficiency decrement could be minimized. At the same time wide bandgap buffer layer and suitable superstrate configuration might extent beneficial effect of model 1.

4 Conclusion

In the present study, we simulated the experimentally observed beneficial and detrimental aspects of light soaking phenomena in thin film solar cells using suitable defect models in SCAPS-1D. Two models utilizing the metastable photo-induced defects of absorber and buffer layers, respectively, are discussed, to numerically replicate the enhancement and degradation in the efficiency of thin film solar cells upon light soaking. A 2D contour plot is generated to show the efficiency dependence on photo-generated defect energy levels and defect densities. We showed that the light soaking in absorber layer is beneficial to overall performance. Photo-induced defects in absorber acts as hole doping thus enhance the built-in voltage. The light soaking in buffer layer is detrimental to the device performance. The photo-induced defects in the buffer causes strong banding within buffer layer and accelerates interfacial recombination, thus lowering the overall performance. Finally, it is suggested that a high bandgap buffer layer or a suitable superstrate structure could passivate detrimental aspect of light soaking associated with the photoconductivity of the buffer layer.

Acknowledgement AK highly acknowledge publisher of SCAPS for providing the package. AK heartily acknowledges his Ph.D. supervisor Dr. Ajay D Thakur for support and guidance during Ph.D. tenure.

References

1. M. Nardone, J. Appl. Phys. **115**, 234502 (2014)
2. F.J. Haug, D. Rudmann, H. Zogg, A.N. Tiwari, Thin Solid Films **431–432**, 431–435 (2003)
3. S. Chen, T. Jarmar, S. Södergren, U. Malm, E. Wallin, O. Lundberg, S. Jander, R. Hunger, L. Stolt, Thin Solid Films **582**, 35–38 (2015)
4. S. Kim, C. Lee, S. Kim, R.B.V. Chalapathy, E.A. Al-Ammar, B.T. Ahn, Phys. Chem. Chem. Phys. **17**, 19222 (2015)
5. H. Yu, W. Lee, J. Wi, D. Cho, W.S. Han, Y. Chung, T. Kim, J. Song, Phys. Chem. Chem. Phys. **18**, 33211 (2016)
6. T. Minemoto, H. Hori, H. Takakaura, Phys. Status Solidi C **6**, 1225–1228 (2009)
7. W. Lee, H. Yu, J. Wi, D. Cho, W.S. Han, J. Yoo, Y. Yi, J. Song, Y. Chung, ACS Appl. Mater. Interfaces. **8**, 22151–22158 (2016)
8. J. Pettersson, C. Platzer-Björkman, M. Edoff, Prog. Photovolt: Res. Appl. **17**, 460–469 (2009)
9. T. Kobayashi, H. Yamaguchi, T. Nakada, Prog. Photovolt: Res. Appl **22**, 115–121 (2014)
10. Gostein M and Dunn L (2011) 37th IEEE Photovoltaic Specialists Conference Seattle, 003126–003131
11. M. Neuschitzer, Y. Sanchez, S. López-Marino, H. Xie, A. Fairbrother, M. Placidi, S. Haass, V. Izquierdo-Roca, A. Perez-Rodriguez, E. Saucedo, Prog. Photovolt: Res. Appl. **23**, 1660–1667 (2015)
12. M. Neuschitzer, K. Lienau, M. Guc, L.C. Barrio, S. Haass, J.M. Prieto, Y. Sanchez, M. Espindola-Rodriguez, Y. Romanyuk, A. Perez-Rodriguez, V. Izquierdo-Roca, E. Saucedo, J. Phys. D Appl. Phys. **49**, 125602 (2016)
13. I. Khatri, K. Shudo, J. Matsuura, M. Sugiyama, T. Nakada, Prog Photovolt Res Appl. **26**, 171–178 (2018)
14. V. Srivastava, S.H. Reddy, M. Mohan, B. Anitha, B. Adara, M.A.G. Namboothiry, J. Phys. D Appl. Phys. **52**, 265302 (2019)
15. Gloeckler M, Sites JR (2004) *19th European Photovoltaic Solar Energy Conference*, 1863–1866
16. S. Leea, K. Price, J. Park, Thin Solid Films **619**, 208–213 (2016)
17. F. Liu, C. Yan, K. Sun, F. Zhou, X. Hao, M.A. Green, ACS Photon. **4**, 1684–1690 (2017)
18. M. Burgelman, P. Nollet, S. Degrave, Thin Solid Films **361–362**, 527–532 (2000)
19. A. Kumar, A.D. Thakur, Curr. Appl. Phys. **19**, 1111–1119 (2019)
20. A. Kumar, A.D. Thakur, Jpn. J. Appl. Phys. **57**, 08RC05 (2018)
21. A. Kumar, A.D. Thakur, AIP Conf. Proc. **1953**, 050022 (2018)
22. S.R. Meher, L. Balakrishnan, Z.C. Alex, Superlattices Microstruct. **100**, 703 (2016)
23. N.M. Mangan, R.E. Brandt, V. Steinmann, R. Jaramillo, C. Yang, J.R. Poindexter, R. Chakraborty, H.H. Park, X. Zhao, R.G. Gordon, T. Buonassisi, J. Appl. Phys. **118**, 115102 (2015)
24. T. Minemoto, M. Murata, J. Appl. Phys. **116**, 054505 (2014)
25. M.O. Reese, C.L. Perkins, J.M. Burst, S. Farrell, T.M. Barnes, S.W. Johnston, D. Kuciauskas, T.A. Gessert, W.K. Metzger, J. Appl. Phys. **118**, 155305 (2015)
26. B. Vermang, V. Fjällström, J. Pettersson, P. Salomé, M. Edoff, Solar Energy Mater. Solar Cells **117**, 505–511 (2013)
27. J. Pettersson, C. Platzer-Björkman, U. Zimmermann, M. Edoff, Thin Solid Films **519**, 7476–7480 (2011)
28. Agostinelli G, Dunlop ED, Batzner DL, Tiwari AN, Nollet P, Burgelman M, Kontges M (2003) *Proceedings of the 3rd World Conference on Photovoltaic Energy Conversion* WCPEC-3 Osaka, pp. 356–359
29. M. Kontges, R. Reineke-Koch, P. Nollet, J. Beier, R. Schaffler, J. Parisi, Thin Solid Films **403–404**, 280–286 (2002)
30. J. Yup, Y. Junggyu, N. Dongseop, K. Dongho, L. Pil, H. Huh, Solar Energy Mater. Solar Cells **144**(467–471), 468 (2016)
31. J. Nishinaga, T. Koida, S. Ishizuka, Y. Kamikawa, H. Takahashi, M. Iioka, H. Higuchi, Y. Ueno, H. Shibata, S. Niki, Appl. Phys. Express **10**, 092301 (2017)

Publisher's Note Springer Nature remains neutral with regard to jurisdictional claims in published maps and institutional affiliations.